Top Curr Chem (2010) 296: 283–304
DOI: 10.1007/128_2010_66

Published online: 2 June 2010

Visualizing Uptake and Intracellular Trafficking of Gene Carriers by Single-Particle Tracking

N. Ruthardt and C. Bräuchle

Abstract Single-particle microscopy und live-cell single-particle tracking are powerful tools to follow the cellular internalization pathway of individual nanoparticles such as viruses and gene carriers and investigate their interaction with living cells. Those single-cell and single-particle methods can elucidate the "black box" between application of the gene carrier to the cell and the final gene expression and allow the essential bottlenecks to be identified in great detail on the cellular level. In this review we will give a short introduction into single-particle tracking microscopy and present an overview of the mechanisms of DNA delivery from attachment to the cell membrane over internalization towards nuclear entry unraveled by single-particle methods.

Keywords DNA/RNA transfection, Fluorescence wide-field microscopy, Gene carriers, Gene therapy, Single-particle tracking, Trajectory analysis

Contents

N. Ruthardt (✉), C. Bräuchle
Department of Chemistry and Biochemistry, Ludwig-Maximilians-Universität München, Butenandtstr. 5-13, 81377 München, Germany
e-mail: Nadia.Ruthardt@cup.uni-muenchen.de
Center for NanoScience (CeNS), Ludwig-Maximilians-Universität München, Butenandtstr. 5-13, 81377 München, Germany

Abbreviations

EGF	Epidermal growth factor
EGFP	Enhanced green fluorescent protein
NGF	Nerve growth factor
PEI	Polyethyleneimide
PLL	Poly-L-lysine

1 Introduction

The delivery of nucleic acids (DNA or RNA) into cells is of central interest for gene therapy in a variety of human diseases including cancer [1]. In order to be transcribed and to exert its intended action, the foreign DNA has ultimately to reach the nucleus of the target cell. In the case of RNA, transport into the nucleus is not necessary as the action of RNA occurs in the cytoplasm (e.g., siRNA). Tissues and cells do not possess special mechanisms for uptake of DNA and several barriers hamper the efficient delivery of the DNA into the nucleus. Those barriers include general obstacles in the body to reach the target tissue after systemic delivery as well as barriers on the cellular level [2]. In order to deliver the DNA, gene carriers (also referred to as gene vectors) have to be used to achieve packaging of the DNA, protection in the body against degradation and eventually specific targeting to the diseased tissue. Currently, two approaches for gene carriers are used: viral and non-viral gene carriers. Several excellent reviews exist for both approaches [3–11]. In this review, we will only discuss non-viral gene carriers. Those artificial carriers have the advantage of a chemically defined synthesis and strongly reduced immune response of the body compared to viral-vectors. However, all currently studied non-viral systems are far less efficient than viral systems based on viruses that have been optimized by natural selection over millions of years. Therefore, one approach to optimize non-viral vectors is to mimic the infection pathway of viruses. In order to do so, the infection pathway of viruses has to be resolved in great detail [12–15] as well as the single steps of the entry pathway of the "artificial viruses" in order to identify the barriers and bottlenecks for gene delivery as a basis for further optimizations [2, 16, 17]. Bulk measurements use the expression of a transgene

as read-out for transfection efficiency, leaving a "black box" for the events between application of the gene carrier to the cell and the final gene expression. Single cell and single-particle methods can elucidate the "black box" and resolve the individual steps of transfection in real time. Thereby, they allow the essential bottlenecks to be identified in great detail on the cellular level that have to be passed once a gene carrier has reached its target cell after systemic administration to the body. Live-cell fluorescence microscopy also has the advantage of including dynamic information on the transfection process as it contains temporal as well as spatial information with high resolution. In this review, we concentrate on single-particle tracking using highly sensitive fluorescence live-cell microscopy for investigation of the transfection pathway in real-time on a single cell level.

2 Investigating the Internalization of Gene Carriers into Cells

Most of the insights into internalization and efficiency of various gene carriers have been obtained by techniques such as flow cytometry and confocal microscopy. Whereas the first is a bulk measurement technique with ensemble averaging of up to several thousand cells and does not provide detailed information on the uptake process on a single cell level, the latter has been used with fixed cells to acquire snapshots of the transfection process on a single cell level. The main optical technique used to study the internalization pathway of gene carriers is multi-color live-cell fluorescence microscopy [18]. Compartments of the endocytic pathway in living cells can be visualized by fluorescently labeled markers (e.g., dye-coupled transferrin, cholera toxin B, or dextrans) or more specifically by cellular expression of marker proteins fused to fluorescent proteins (e.g., clathrin-GFP, caveolin-GFP) [19]. The entry of gene carriers labeled with a fluorescent dye can then be followed in the living cell and colocalization analysis with cellular compartments labeled with another fluorescent dye provides information about the route taken. This method can be extended by using chemical inhibitors or siRNA for specific entry pathways to test whether the internalization of gene carriers can successfully be blocked. However, the use of markers and inhibitors at the single cell level has some caveats [20]. Based on those techniques, it was revealed that all tested gene carriers enter cells by endocytosis [21–23], and also those connected to cell penetrating peptides [24–26]. However, there is no generalized internalization pathway for gene carriers. The exact endocytic pathway used by gene carriers is strongly dependent on the individual cell type and also the sort of gene carrier [21, 27]. Often, several endocytosis pathways are used simultaneously and inhibition of one pathway may increase the internalization by an alternative route. In addition, the pathway finally resulting in successful gene expression varies with cell line and also gene carrier type [27]. Therefore, the knowledge of the exact internalization pathway of a specific gene carrier is required to improve its efficiency. One approach to increase transfection efficiency is to predefine a pathway leading to successful gene expression by targeting to a specific receptor.

This can concomitantly be connected to cell specific targeting [28–31]. However, the exact entry pathway has to be defined for each target cell line and particle type individually. The possibilities of traditional confocal microscopy as described above to extract dynamic information are limited. A relatively new technique to investigate the dynamic process of transfection in detail is the tracking of single gene carriers in real-time in living cells to obtain spatial as well as temporal information with high resolution.

3 Single-Particle Tracking Microscopy

3.1 Microscope Set-Up

Single-particle techniques using highly sensitive fluorescence wide-field microscopy reveal the internalization process on short time scales and in great detail. This allows continuous observation of the internalization of single gene carriers, starting with their attachment to the cell membrane, followed by individual steps of the uptake process and intracellular trafficking. Imaging of single gene carriers eventually labeled with a few fluorophores at high temporal resolution over several minutes requires highly sensitive detection methods. Typically, these highly sensitive microscopes are custom-built and based on an inverted microscope (Fig. 1). Excitation is performed by laser light which provides the necessary excitation intensity required for strong photon emission by the fluorophores. Typical laser lines are 488, 532, 561, and 635 nm for excitation of common fluorophores. The availability of several laser lines allows simultaneous imaging of two to three fluorophores, depending on emission spectra of the labels and filters available. The aligned laser light is guided into the back of the objective by optics such as mirrors, dichroic mirrors, lenses, and optical fibers. Acousto-optical tunable filters (AOTFs) allow selecting the appropriate excitation laser without speed limitations or vibrational and mechanical constrains related to mechanical shutters or rotating wheels. In addition, they can easily accommodate several laser lines at different output wavelengths. The cells are kept at 37°C throughout the experiment by a temperature controlled stage (heating table). As oil immersion objectives are in direct contact with the cover glass surface where the cells are grown, they act as a strong heat sink for the cells. Hence, it is necessary to heat the objective to 39°C and an adjustable correction collar is needed to correct the optics for the higher temperature. There are also microscope stage incubator chambers available for adjusting the CO_2 level, but with the exception of long-time experiments, the use of CO_2-independent medium is sufficient. Focal instabilities in the microscope mechanics due to temperature changes in the surroundings after mounting the sample are major troubles for single-particle tracking. An auto-focus system is advantageous and keeps the sample at a constant z-position. The emission light is typically collected by 60× or 100× oil immersion objectives with high numerical

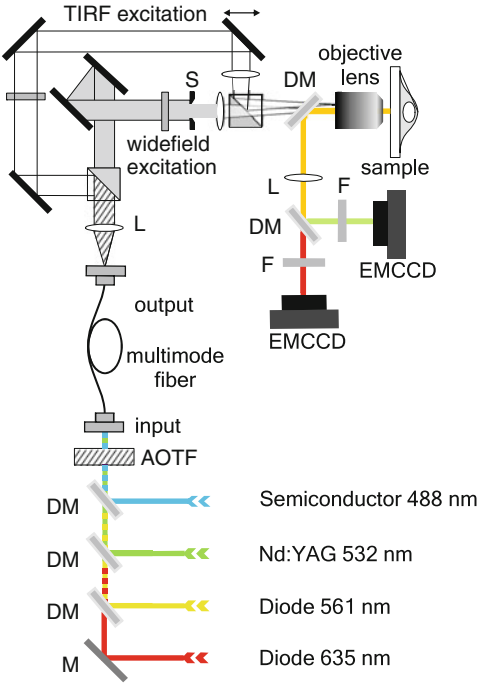

Fig. 1 Schematic drawing of a wide-field single-particle tracking fluorescence microscope equipped. Several lasers are used as excitation source for different fluorophores with fast selection by an acousto-optical tunable filter (AOTF). The collimated laser light is coupled into the objective such that only the observed area is illuminated. The emission light is separated from the excitation light by a dichroic mirror. In the case of multi-color imaging, the emission light is separated by a second dichroic mirror and the two emission channels are detected on EM CCD cameras. As an option, the excitation path can alternatively be switched by a beam splitter to total internal reflection illumination (TIRF) for imaging of processes close to the coverslip, e.g., the basal cellular plasma membrane. *DC* dichroic mirror, *M* mirror, *L* lens, *S* slit, *F* filter. Adapted with permission, courtesy of Dr. Sergey Ivanchenko

aperture up to 1.49 NA and separated from the excitation light by appropriate dichroic mirrors depending on the fluorophores used. The fluorescence emission is then directed to and detected by a highly sensitive and fast electron multiplied charge-coupled device (EM CCD) camera. For multi-color imaging, the use of two separate cameras for detection instead of simultaneous illumination of the two halves of a single camera chip increases the field of view and combinatorial possibilities of multiple fluorophores for labeling, but also increases the cost of the set-up substantially. The exact configuration of the set-up, mainly the choice of lasers, dichroic mirrors, and filters, depends on the combination of fluorophores used and may have to be adapted for the individual experiments by the user. Also accessory optics like total internal reflection fluorescence microscopy (TIRFM) illumination (see Fig. 1) or confocal detection can be added to increase the flexibility and variability of custom-built set-ups. TIRF illumination is especially interesting for fast tracking of cell surface associated events at the basal plasma membrane.

3.2 Trajectory Analysis and Mean-Square Displacement Plots

In the acquired image sequences, the fluorescent particles can be identified as bright spots on a dark background. Each frame in the movie is a representation of the position of the particles at a certain time point. By extraction of the x and y coordinates of the particles derived from the centroids of their diffraction limited spots in all frames of the movie, the trajectories of the particles can be obtained. This is typically performed by a particle-finding algorithm that first reduces background noise and then selects particles by setting an intensity threshold of the filtered image in the first round. In the second round, particles for tracking are selected based on their intensity and size. The x and y coordinates are obtained by fitting a 2D-Gaussian function to the particle's intensity profile (Fig. 2a). The particle coordinates are subsequently used for calculating the corresponding trajectories based on a nearest-neighbor algorithm [32, 33]. With this method, a positional accuracy well beyond the optical diffraction limit can be achieved. The centroid position of a sufficiently bright fluoropore can be determined with nanometer precision [34]. Thus, trajectories can be generated that are well below the resolution of light microscopes and impressively demonstrate the power of single-particle tracking.

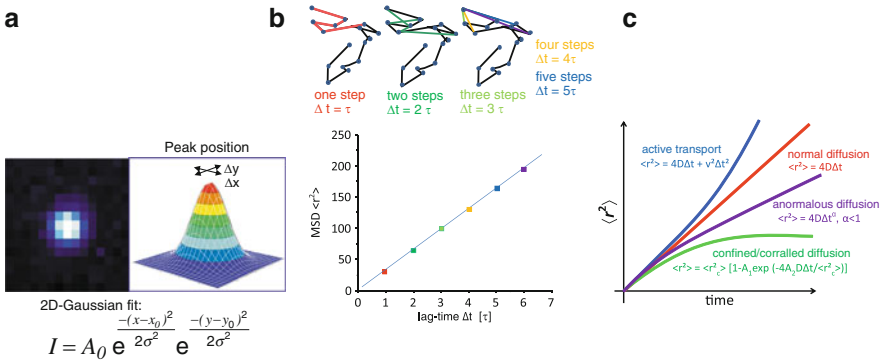

Fig. 2 Positional detection and mean-square displacement (MSD). (**a**) The x, y-coordinates of a particle at a certain time point are derived from its diffraction limited spot by fitting a 2D-Gaussian function to its intensity profile. In this way, a positional accuracy far below the optical resolution is obtained. (**b**) The figure depicts a simplified scheme for the analysis of a trajectory and the corresponding plot of the time dependency of the MSD. The average of all steps within the trajectory for each time-lag Δt, with $\Delta t = \tau, \Delta t = 2\tau, \ldots$ (where τ = acquisition time interval from frame to frame) gives a point in the plot of MSD = f(t). (**c**) The time dependence of the MSD allows the classification of several modes of motion by evaluating the best fit of the MSD plot to one of the four formulas. A linear plot indicates normal diffusion and can be described by $<r^2> = 4D\Delta t$ (D = diffusion coefficient). A quadratic dependence of $<r^2>$ on Δt indicates directed motion and can be fitted by $<r^2> = v^2\Delta t^2 + 4D\Delta t$ (v = mean velocity). An asymptotic behavior for larger Δt with $<r^2> = <r_c^2>\,[1 - A_1 \exp(-4A_2 D\Delta t/<r_c^2>)]$ indicates confined diffusion. Anomalous diffusion is indicated by a best fit with $<r^2> = 4D\Delta t^{\alpha}$ and $\alpha < 1$ (sub-diffusive)

The resulting trajectories are usually analyzed for the mode of motion executed by the particle as the motion provides information on the location and status of the particle as described in this review. The most common analysis starts with the calculation of the so-called mean-square displacement (MSD). Then, the time dependence of the MSD is plotted. This plot allows a mode of motion analysis [35]. A simplified way to calculate the MSD is depicted in Fig. 2b. The mean square displacement $<r^2>$ describes the average of the squared distances between a particle's start and end positions for all time-lags of certain length Δt within one trajectory.

With increasing time-lag, however, the uncertainty of the MSD values increases. When the calculated time-lag becomes a substantial fraction of the total points of the trajectory, there are not enough pairs of data points for an accurate calculation of the MSD as shown by the formulas for the standard deviation [36]. To account for this uncertainty, the MSD should always be calculated for time-lags corresponding to only about one quarter of the total number of points in the trajectory [35]. So, for example, in a trajectory with 800 data points, the MSD is calculated only for time-lags spanning a maximum of 200 points. As a consequence, the time-axis of an MSD plot can only represent a fraction of the time scale of the trajectory. From evaluation of the MSD plot, information about the mode of motion can be obtained (Fig. 2c). This mode of motion can then be interpreted in a biological context and conclusions on the location and environment of the tracked particle can be drawn.

Normal and anomalous diffusion is described by

$$\left\langle r^2 \right\rangle = 4D\Delta t^{\alpha}, \tag{1}$$

where D is the diffusion coefficient. The factor 4 is specific for diffusion in two dimensions. For normal diffusion (Brownian motion), $\alpha = 1$ and a linear dependence of $<r^2>$ on the time interval Δt is given. Anomalous diffusion is described by $\alpha < 1$ and is typically observed, when the diffusive particle is hindered by obstacles.

Confined or corralled diffusion is indicated by an asymptotic behavior of $<r^2>$ for large Δt and implies a confinement for the diffusive particle. The following formula describes the relation between $<r^2>$ and Δt:

$$\left\langle r^2 \right\rangle = \left\langle r_c^2 \right\rangle \left[1 - A_1 \exp\left(-4A_2 D\Delta t / \left\langle r_c^2 \right\rangle\right)\right]. \tag{2}$$

$<r_c{}^2>$ is an approximation of the size of the confinement and the constants A_1 and A_2 are determined by the confinement geometry. The asymptotic value of $<r^2>$ for large Δt, which is independent of the confinement geometry, can be taken for the calculation of the size of the confinement $<r_c{}^2>$. We note that confinement within a certain region can only be observed when the observation time is long compared to the time between successive contacts of the particle with the barrier. For short observation times, normal or anomalous diffusion within the confinement is observed.

Active transport is described by a quadratic dependence of the mean square displacement $<r^2>$ on Δt with

$$\left\langle r^2 \right\rangle = v^2 \Delta t^2 + 4D\Delta t. \tag{3}$$

v is the velocity of the directed motion which is also called drift. Superimposed on this motion is a normal diffusion with the diffusion coefficient D. The whole process can be described with the picture of a conveyor belt, where particles are transported but can also diffuse to both sides as well as along the belt. By fitting (3) to an MSD curve, the mean velocity v of the directed motion and the diffusion coefficient D are obtained.

MSD curves of diffusive motion can be very heterogeneous (Fig. 3) and it has to be tested which of the models for diffusion results in a higher correlation coefficient for the fitted plot.

4 Single-Particle Tracking of Gene Carrier Internalization

Combining sensitive fluorescence wide-field microscopy and single-particle tracking, de Bruin and coworkers followed the internalization process of single polymeric gene carriers (polyplexes) in real time in living cells with a temporal resolution of 300 ms [37]. In trajectories showing the full internalization process of epidermal growth factor receptor (EGFR)-targeted polyplexes starting with attachment to the cell membrane followed by uptake into the cell and finally active transport towards the nucleus, they typically found three phases of motion (Fig. 3, the video corresponding to the trajectory can be found in the supplemental material of [37]). Phase I showed slow directed motion, phase II consisted either of normal, anomalous, and confined diffusion or a combination of them, and finally phase III showed fast active transport in the cytoplasm. Shortly after attachment to the cell membrane, the polyplexes started a slow directed transport during phase I with velocities of typically 0.01 μm/s. This transport was attributed to the movement of the underlying actin cytoskeleton mediated by the EGF receptor and linker proteins as revealed by dual-color microscopy. The polyplexes were thus transported by the retrograde actin flow within the cell. A similar behavior was also observed for untargeted polyplexes by Bausinger et al. [38], where the cell-surface attached polyplexes colocalized with actin fibers of the underlying cortical actin network. In these experiments, single-particle tracking of the membrane bound polyplexes revealed a variety of motion behavior including 2D free diffusion, anomalous diffusion as well as complete immobilization. In addition, slow active transport around 0.01 μm/s typical for actin mediated transport was observed at later stages. For untargeted cationic gene carriers, cell-surface proteoglycans such as heparan sulfate proteoglycans (HSPGs) have been suggested as a kind of “unspecific receptor” with binding characteristics based on electrostatic interactions [23, 39].

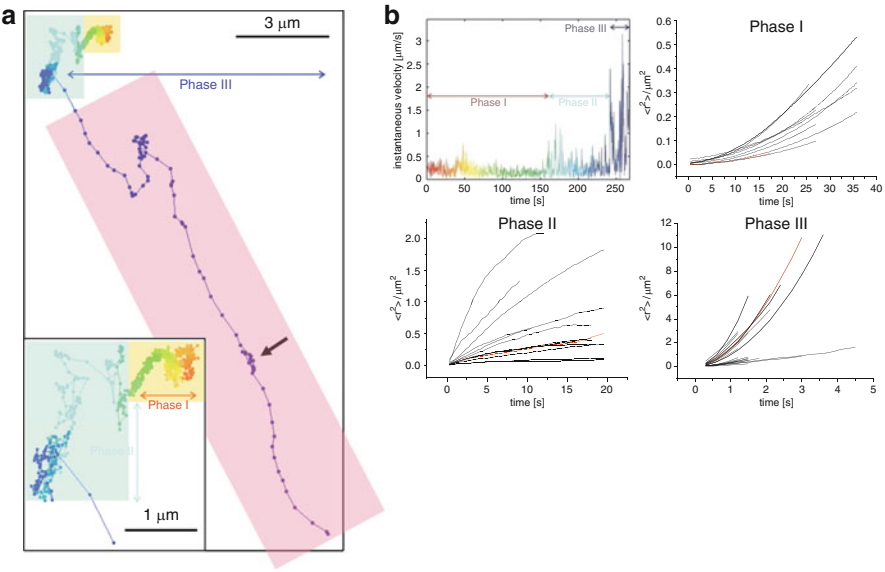

Fig. 3 Single-particle tracking of the internalization of an epidermal growth factor receptor (EGFR)-targeted polyplex. (**a**) Trajectory of a polyplex incubated on a HuH7 cell. The particle was tracked for 4 min and 30 s at a temporal resolution of 300 ms and the trajectory displays the three phases typically observed during internalization. The trajectory starts immediately after the polyplex attached to the cell membrane. The color of the trajectory is shown as changing from red to blue-violet with progressing time and matches the corresponding velocity plot in (**b**). The *arrow* indicates a spot of back-and-forward movement. The corresponding video is available as supplemental information in [37]. The *overlaying color boxes* mark the phases: *yellow*: phase I – slow active transport, *blue*: phase II – anomalous and confined diffusion, *purple*: phase III – active transport. (**b**) Instantaneous velocity plot of the trajectory shown in (**a**) and MSD plots of the three phases analyzed from several trajectories. The plots corresponding to the trajectory presented in panel (a) are drawn in *red*. Based on (1), the mean drift velocity for all plots in phase I was $v_I = 0.015$ μm/s and the corresponding diffusion coefficient $D_I = 4 \times 10^{-4}$ μm^2/s. For phase II, the plots could not be averaged due to heterogeneous appearance showing anomalous, normal and confined diffusion. In case of confined motion, the confinement diameters calculated from the information provided in (2) ranged from 0.3 to 2.0 μm. The values for α in anomalous diffusion ranged from 0.4 to 0.7. Phase III plots show a quadratic dependence of $<r^2>$ on Δt indicating directed motion. The mean velocity for the presented trajectories was calculated as $v_{III} = 0.7$ μm^2/s with a corresponding mean diffusion coefficient of $D_{III} = 0.1$ μm^2/s. Adapted with permission from the American Society of Gene Therapy [37]

The results of the single-particle tracking from Bausinger et al. support the model of receptor binding by the polyplexes and receptor clustering before endocytosis occurs. Recent experiments using colocalization with fluorescent markers, inhibitor, and siRNA treatment by Payne [40] provides strong evidence for proteoglycans as the unspecific receptors for polyplexes. Targeting gene carriers to specific cell surface receptors can influence the internalization behavior. De Bruin [37] and coworkers demonstrated in their study that targeting of polyplexes to the EGF receptor leads to increased and accelerated endocytosis of the polyplexes. Instead of

the unspecific proteoglycan mediated endocytosis, the polyplexes were quickly internalized by the specific EGF receptor mediated endocytosis. The fast endocytosis was represented in the trajectories by strongly shortened time spans of phase I motion.

The internalization event itself – namely the pinching off of an endocytic vesicle from the plasma membrane – cannot be resolved by light microscopy. However, by combining single-particle tracking with fluorescence quenching of extracellular polyplexes at different time points, de Bruin et al. [37] showed that the internalization into an endocytic vesicle occurs during phase I. More interestingly, some polyplexes defined as intracellular continued the slow directed movement characteristic for phase I for a certain time before entering the movement characteristic for intracellular particles. They suggested that the newly formed endocytic vesicles close to the membrane may be trapped in the cortical actin cytoskeleton and therefore show motion similar to the polyplexes bound to the membrane and connected to the actin cytoskeleton by transmembrane proteins.

5 Types of Intracellular Movement

After internalization in phase I, most polyplexes show anomalous or confined diffusion (phase II) followed by active transport (phase III) [37]. The anomalous diffusion and confinement displayed by the MSD analysis represent the local microenvironment of the particles in the cytoplasm where the cytoskeleton, organelles and large macromolecules are local obstacles for free diffusion. Suh et al. [41] tracked internalized polyplexes with a temporal resolution of 33 ms and found diffusive motion of polyplexes where the corresponding trajectories showed hop diffusion (Fig. 4). These hop diffusion patterns can be interpreted as the cages of the

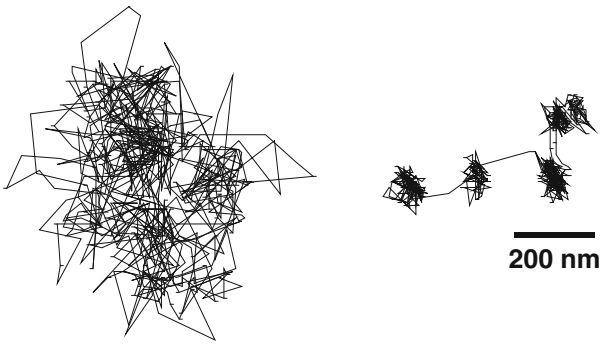

Fig. 4 Example trajectories of diffusive (*left*) and subdiffusive (*right*) gene carriers recorded with a temporal resolution of 33 ms. The subdiffusive trajectory is characterized by confined motion in the MSD plot. However, the hop diffusion pattern of the trajectory can only be detected by its morphological pattern and not by the shape of MSD plot. Adapted with permission from the American Chemical Society and American Institute of Chemical Engineers [41]

local microenvironment or may even represent the attachment of the vesicles to subcellular structures followed by detachment.

Long range active transport occurs with motor proteins (kinesins or dyneins) along microtubules with velocities up to 4 μm/s and is a feature of internalized particles. Typically, this long range active transport displays the so-called stop-and-go motion as a result from binding and unbinding of motor proteins to the microtubules [37, 41, 42]. Reversal of the transport direction can frequently be observed (see arrow in Fig. 3). In addition to active transport along microtubules, active transport in the cytosol can also occur by so-called actin comet tails. In contrast to active transport by motor proteins, this type of movement is generated by polymerization of actin behind the moved cargo without involvement of motor proteins [43]. The resulting force is used for example, by bacterial pathogens for movement in infected host cells as well as for transport of organelles within the cell. De Bruin et al. observed active transport of endosomes containing polyplexes by actin tails (see supplementary video in [37]). Merrifield et al. tracked endosomes moving by actin tails with a velocity of 0.24 ± 0.10 μm/s [44]. With single-particle tracking, it can be detected by dual-color microscopy with simultaneous imaging of fluorescently labeled actin in order to identify actin tails correlating with active movement.

It has to be noted that the detection of the various diffusive states as well as active transport depends on the time scale of observation. For short time scales, the short-range motion of tracked particles may seem similar and indicates the same local microenvironment for the particles as it is dominated by Brownian motion [37, 41]. Confined diffusion as well as active transport require a minimal duration for detection and appear at longer time scales (see MSD plot). To display confined diffusion, the particle has to experience the boundaries of confinement in its local microenvironment which restrict the free diffusion on longer time scales. Similarly, for active transport, the second part of (3) $4D\Delta t$ is predominant on short time scales. The active transport component $v^2\Delta t^2$ becomes dominant at longer observation periods.

In addition, to detect the various types of motion displayed by a moving particle within a trajectory, the MSD must be taken over subregions of the trajectory. Otherwise, the MSD over the full trajectory would result in an averaging effect over all modes of motion. The careful description of the various modes of motion within one trajectory requires the separation of the trajectory in several parts, e.g., manually according to morphological differences or by velocity thresholds [37, 41]. A careful trajectory analysis also includes a morphological analysis of the trajectory pattern and should include more information than the shape of the MSD or effective diffusion coefficient curves. Particles showing hop diffusion may fulfil all analysis criteria for "diffusive" motion whilst the hop diffusion pattern is only visible in the trajectory [41].

A more sophisticated method for automated trajectory analysis and mode of motion detection provides the use of a rolling-window algorithm. The algorithm described by Arcizet et al. [45, 46] reliably separates the active and passive states of particles and extracts the velocity during active states as well as the diffusion coefficients during passive states (Fig. 5). It takes into account that active transport by microtubules is characteristically directional over a certain time and measures

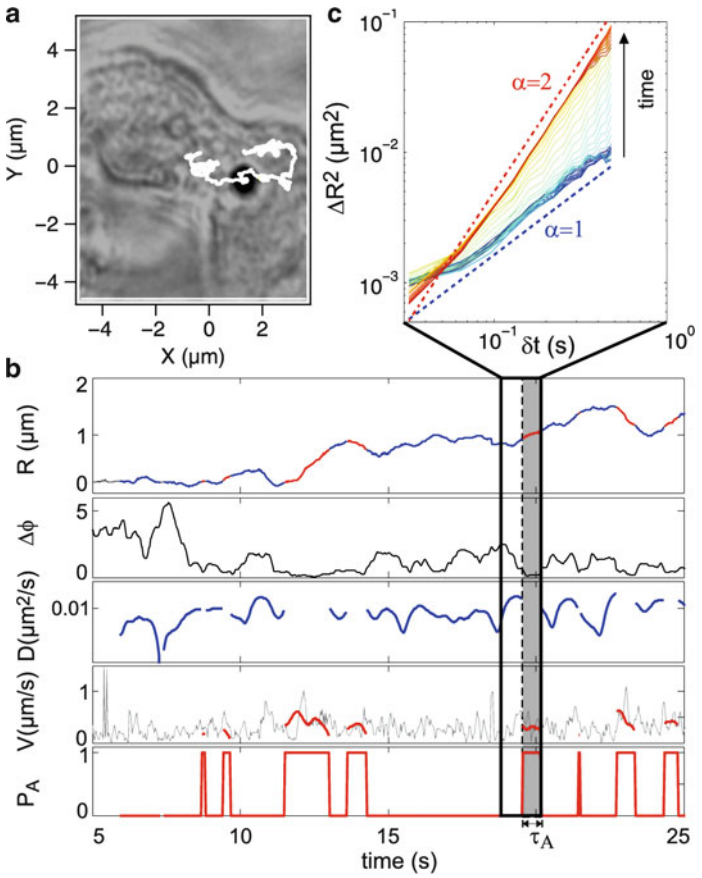

Fig. 5 Trajectory analysis with an automated rolling-window algorithm for detecting active transport and diffusive phases of motion. (**a**) Analyzed trajectory of an internalized microbead overlayed onto the transmission image of the cell. (**b**) The rolling-window algorithm analysis of the trajectory with, from the top to the bottom, displacement *R(t)* with diffusive (*blue*) and active (*red*) phases, standard deviation $\Delta\phi$ of the angle correlation function, diffusion coefficient *D(t)* retrieved during the diffusive states, instantaneous velocity (*light grey*) and algorithm-retrieved velocity during the active phases (*red*), and the binary state variable P_A for active motion probability. The *shaded* part of the frame highlights an active phase. (**c**) Examples of local MSD calculated with fits to (1) with trends for $\alpha = 1$ (normal diffusion, *blue dotted line*) and 2 (active transport, *red dotted line*). Reproduced with the permission from the American Physical Society [46]

the directional persistence of particle motion by the angular correlation of following steps by an angle correlation function [46] resulting in an estimate of the probability of the particle undergoing active motion within the analyzed subregion. Of course, the higher the temporal resolution and the more data points acquired, the better and more detailed the analysis can be. As a consequence, for very fast transport events, the temporal resolution has to be high enough to acquire sufficient data points for analysis and separation between modes of motion.

6 Defining the Endosomal Pathway by Its Motion Characteristics

As gene carriers are internalized by endocytosis, the motion characteristics inside the cell resembles the movement of the endosomal compartments within the cell and the formed vesicles are transported along the microtubule network [38]. Suh et al. [41] quantified the transport of individual internalized polyplexes by multiple-particle tracking and showed that the intracellular transport characteristics of polyplexes depend on spatial location and time posttransfection. Within 30 min, polyplexes accumulated around the nucleus. An average of the transport modes over a 22.5 h period after transfection showed that the largest fraction of polyplexes with active transport was found in the peripheral region of the cells whereas polyplexes close to the nucleus were largely diffusive and subdiffusive. Disruption of the microtubule network by nocodazole completely inhibits active transport and also the perinuclear accumulation of polyplexes [37, 40, 47].

Sauer et al. [48] investigated the internalization of magnetic polyplexes with single-particle tracking. Magnetic particles can be directed within the body to the diseased tissue by application of a magnetic field. On the single cell level, the three-phased internalization behavior was also observed for these particles and was found to be independent of the applied magnetic field. Therefore, the application of a magnetic field affected only extracellular magnetic polyplexes and concentrated these particles onto the plasma membrane whereas the cellular processes of uptake and trafficking were unaffected.

The three phases described by de Bruin et al. [37] for the internalization of polyplexes were also found in a study of endocytic trafficking of single receptors by Rajan et al. [49]. They took advantage of the extraordinary features of quantum dots (QDots) to follow the internalization of single nerve growth factor (NGF) receptors by single-particle tracking on the single protein level at 79 ms temporal and nanometer-scale spatial resolution. QDots are fluorescent semiconductor nanocrystals with tunable fluorescence emission dependent on their size. They are extremely bright with extraordinary photostability. The emission spectrum shows a characteristic narrow peak, making it favorable for multi-color applications. Common fluorescent dyes such as Alexa, Cyanine, or Atto dyes suffer from fast bleaching and limited signal-to-noise ratio against the autofluorescence background of living cells. This is especially critical in cases where labeling at single molecule ratio is required [15]. The photophysical properties of the labeling dyes are then critical for sufficiently long tracking to obtain meaningful trajectories. A drawback of QDots is their blinking behavior, which, on the other hand, can be used to discriminate between single QDots and aggregates. By tracking the endocytosis of single labeled receptors by QDot-NGF, Rajan et al. demonstrate that the distinct phases of motion reflect the underlying phases of endocytosis which are regulated with a high degree of uniformity. Once endocytosed, the receptor-QDot-NGF complexes did not show much variation and their dynamics are correlated with the type of the endosomal compartment. By tracking the internalization of QDot-NGF complexes in neurons

at 10 frames/s, Cui et al. investigated the long range motion characteristic of endosomes in axons [42]. Within the axons, single QD-NGF containing endosomes showed active transport along microtubules with typical stop-and-go motion towards the cell body. Interestingly, their study showed that the average speed of endosomal movement varied considerably between axons and suggests that the ability to support endosomal traffic may differ between individual axons. The superior optical properties of QDots compared to conventional organic fluorophores even allow the detection of individual microtubule motor steps in living cells. By tracking endocytosed QDots with an extremely short temporal resolution of 300 μs, Nan et al. [50] resolved individual 8 nm steps taken by endosomes traveling with a velocity of about 3 μm/s.

7 Endosomal Release of Gene Carriers

In order to reach the nucleus, DNA intended for transfection has to escape the endosome and be released from the carrier. Currently, this is a major bottleneck of non-viral gene carriers [22, 51]. To optimize the overall efficiency of transfection, the mechanism of endosomal release utilized by current gene carriers is being investigated but is not yet fully understood. For PEI – the polymer with the highest transfection efficiency – two hypotheses for its release are discussed: first, the proton-sponge effect and second the membrane destabilizing effect [52]. The first hypothesis is based on the high buffering capacity of PEI accompanied by an increased chloride accumulation resulting in osmotic swelling of the endosome [53], the second model by binding of PEI to the membrane [54]. An approach to increase endosomal escape is the use of membrane destabilizing peptides [55, 56]. Generally, the release of gene carriers may be a slow and transient process occurring at different times for each endosome. To image the endosomal escape and DNA release behavior of different polyplex compositions with varying polymers on a single vesicle level, de Bruin et al. took advantage of the possibility of inducing release of internalized double-labeled polyplexes photochemically using laser light [57]. In this technique, endosomal membranes were loaded with a photosensitizer that was activated by a 405 nm laser pulse to produce singlet oxygen resulting in the rupture of endosomal membranes and release of the endosomal content. By imaging the release process of single endosomes at high temporal resolution, they showed that the release of the DNA is dependent on the polymer used for complexation. After rupture of the endosomal membrane, escape of the content occurred on a millisecond time scale. In the case of polyplexes based on PEI and DNA, the fluorescence signal of the labeled PEI vanished in less than 1 s due to diffusion into the cytosol. The fluorescence signal of the labeled DNA, in contrast, remained at the location of the ruptured endosome (Fig. 6). As DNA molecules larger than ~1,000 bp cannot diffuse within the crowded cytoplasm [58], released plasmid DNA is basically immobile in contrast to the smaller sized polymer. However, the DNA was protected from degradation until endosomal rupture occurred and

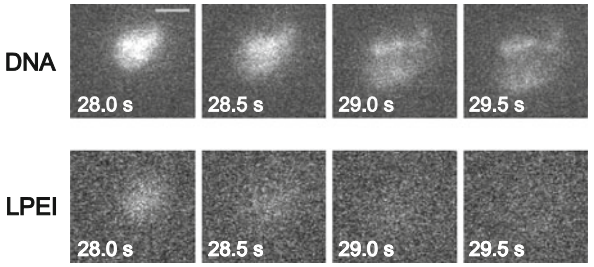

Fig. 6 Endosomal release of PEI/DNA polyplexes. Rupture of a single endosome filled with polyplexes consisting of DNA and PEI labeled by different fluorophores. The *upper panel* shows the DNA signal and reveals that the intact DNA remains in a confined area of the damaged endosome without diffusion in the cytosol. The *lower panel* shows the polymer signal whose fluorescence signal disappears due to diffusion into the cytosol. *Scale bar*: 2 μm. Reproduced with permission from Elsevier B.V. [57]

successfully released from the PEI. For polyplexes composed of PLL and DNA, the endosomal escape was different. The DNA remained either tightly bound to the polymer or vanished quickly by diffusion simultaneously with the polymer due to degradation within the endosome before its rupture. How the DNA molecules get into the nucleus after release is still unclear. There is evidence that plasmid DNA can be trafficked in the cytosol along microtubules. The DNA interacts with microtubules most likely through cytosolic adaptor proteins as demonstrated by Vaughan and Dean [59] using a microtubule spin-down assay. They also showed that microinjected plasmid DNA accumulates around the nucleus after 5 h over distances that are unlikely for free diffusion. However, active transport of free plasmid DNA in the cytoplasm has not been shown yet.

This is in contrast to viruses, where the virus particles also show active transport when present in the cytosol after fusion with the plasma membrane or endosomal membrane [60–62]. This is due to the ability of specific proteins of the virus particle to bind motor proteins. Single-particle tracking reveals that the quantitative intracellular transport properties of internalized non-viral gene vectors (e.g., polyplexes) are similar to that of viral vectors (e.g., adenovirus) [63]. Suk et al. showed that over 80% of polyplexes and adenoviruses in neurons are subdiffusive and 11–13% are actively transported. However, their trafficking pathways are substantially different. Polyplexes colocalized with endosomal compartments whereas adenovirus particles quickly escaped endosomes after endocytosis. Nevertheless, both exploit the intracellular transport machinery to be actively transported.

8 Nuclear Entry of Transgenes

The detection of gene carriers in the nucleus by optical methods is controversially reported. Some studies report the presence of gene carriers in the nucleus [64–66], in others the presence of gene carriers was not detected in the nucleus [22, 54, 67,

68]. It is also unclear whether complete particles can actually enter the nucleus. A possible scenario for polyplexes to enter the nucleus is during mitosis when the breakdown of the nuclear envelope occurs. Polyplexes have been shown to move along the astral microtubules of the mitotic spindle apparatus [38] and it was shown that mitosis increases the rate of successfully transfected cells [69–72]. In most studies the evidence for transgenic DNA in the nucleus is given indirectly by the expression of the transgene. One reason for the difficulty to detect transgenic DNA in the nucleus by optical methods is that the number of DNA molecules finally reaching the nucleus is very small compared to the amount of DNA added to the cells. By using quantitative PCR, Cohen et al. found 75 and 50,000 plasmids per nucleus for B16F10 cells and A549 cells (which scaled to only 1 and 5% of the applied dose). Interestingly, lipoplex-delivered plasmids were more efficiently expressed than polyplex-delivered plasmids, indicating that PEI may remain bound to the DNA and render it transcriptionally inactive. It also seems that there is an upper limit for gene expression as any increase above 3,000 plasmids per nucleus resulted only in marginal increase in expression of the transgene as demonstrated by Cohen et al. [73].

Whether the components of the gene carriers actually remain associated during import into the nucleus or enter individually cannot be answered by optical methods as their resolution is limited. A possible technique to study the complexation of DNA within cells is fluorescence correlation spectroscopy (FCS). Clamme et al. studied the intracellular fate of PEI after transfection with polyplexes by two-photon fluorescence FCS [54]. They showed that PEI binds to the inner membrane of endosomes and lysosomes and shows free diffusion in the cytosol as well as the nucleus. However, they did not detect any PEI/DNA complexes inside the nucleus.

Expression studies combined with mathematical modeling of transfection indicates that actively transcribed plasmids after poly- or lipoplex mediated transfection may be even as low as around three plasmids per nucleus [72]. As a consequence, tracking the entry of DNA which is finally transcribed into the nucleus in living cells with optical methods resembles the search for the needle-in-the-haystack. As described above, single-particle tracking certainly provides the possibilities to track a single labeled plasmid during the transfection cycle. However, as only a few percent of the plasmids actually reach the nucleus, the background of internalized labeled DNA may hinder the detection of the few plasmids actually entering the nucleus.

9 Future Techniques: Going to the Third Dimension

Most single-particle tracking studies are performed in x, y and therefore represent a 2D projection of the real movement. Particles apparently immobile in x, y can actually show movement along the z-axis and a 2D analysis would provide misleading results. Particles moving several microns along the z-axis will usually be completely lost during tracking as they move out of the focal area. Confocal

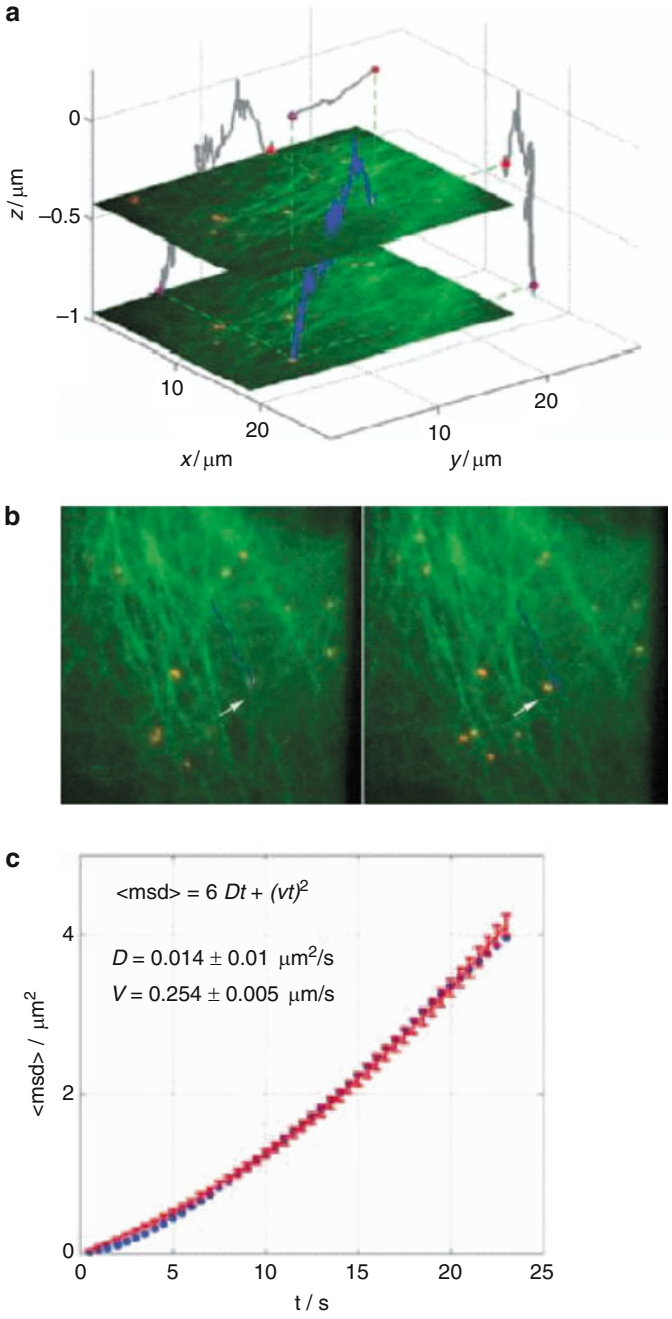

Fig. 7 3D orbital tracking of a polyplex inside a cell(**a**) The 3D trajectory (*blue*) of a polyplex was tracked in HuH7 cells with EGFP labeled tubulin (green structures in the image). Overlayed onto the 3D trajectory are two wide-field images taken at different z-positions during the measurement.

microscopes such as laser scanning or spinning disk microscopes also allow sampling of the z-axis. The acquisition of z-sections, however, is time consuming and usually results in a temporal resolution too slow for detection of fast movement. To extend the capabilities for 3D analysis with a conventional wide-field microscope, Holtzer et al. [74] introduced a cylindrical lens into the emission pathway to produce axial astigmatism. The resulting ellipticity was used to calculate the z-position of small objects with a positional accuracy of 40 nm lateral and 90 nm axial. With this set-up, they were able to track endocytosed QDots at an interval time of 50 ms in three dimensions. An alternative 3D single-particle tracking approach was developed by Katayama et al. [75]. They used a confocal orbital tracking approach with feedback loop for tracking in real time during recording. With this method, the orbiting laser beam is kept centered on the tracked particle. By using two planes for the confocal detection, one above the particle and one below, the z-position of the particle is detected. The orbit is centered on the particle by an online feedback algorithm. In addition, a concomitantly recorded wide-field image in a second channel shows the local environment. This technique allows fast tracking with a temporal resolution down to 16 ms and tracking accuracy of $\sim$20 nm in lateral and 60 nm in axial directions. Due to the simultaneous wide-field imaging, both methods can be used to determine the lateral position of the particle as the particle is kept in focus by the feedback algorithm. With this method, Katayama et al. tracked internalized polyplexes in enhanced green fluorescent protein (EGFP)-tubulin labeled cells (Fig. 7). They showed active transport along microtubules, which were detected in the wide-field channels, with considerable motion along the z-axis as revealed by the 3D trajectory recorded by the confocal channel. However, confocal 3D tracking is limited in terms of multiple-particle tracking.

10 Conclusion and Outlook

Single-particle tracking in real time is a powerful technique to follow the entry pathway of gene carriers as well as their intracellular fate in great detail. The development of nanoparticles as gene carriers will continue and further functionalities such as specific targeting, redox- or pH-sensitivity, etc., will be added. This will lead to even smarter carrier systems [76]. Such systems are constructed to

Fig. 7 (continued) 2D projections of the 3D trajectory are shown in *gray* on the respective axes. (**b**) Two frames of the wide-field movie that was concomitantly recorded during orbital tracking of a polyplex (*red dots*). The wide-field movie allows the correlation of motion events with cellular structures such as microtubules (*green*). (**c**) MSD plot (*blue curve*) of the blue trajectory presented in (**a**). The plot is fitted (*red curve*) with $<r^2> = v^2\Delta t^2 + 6D\Delta t$ in contrast to (3), as the factor 6 is specific for diffusion in three dimensions.Reproduced with permission from Wiley-VCH [75], courtesy of Prof. Don C. Lamb

follow a defined sequence of steps to exert special functions at specific locations in the cell. Single-particle microscopy offers the possibility to follow the action of those smart carrier systems in real time and visualize their correct or incorrect behavior on the cellular level. By combining single-cell single-particle techniques with imaging of the systemic pathway in the living animal [77], it will be possible to follow the full pathway of a single-particle from the point of application in the body throughout the whole animal to the target tissue and subcellular point of action. Thus, the combined possibilities of the various techniques will allow unraveling of the full picture of the "infection pathway" of gene carriers and detection of the critical steps for further optimization to the ultimate goal of a fully functional "artificial virus".

Acknowledgments This work was supported by the Nanosystems Initiative Munich (NIM) and the Center for Integrated Protein Science Munich (CiPSM) and the SFB 749.

References

1. Verma IM, Weitzman MD (2005) Gene therapy: twenty-first century medicine. Annu Rev Biochem 74:711–738
2. Read ML, Logan A, Seymour LW (2005) Barriers to gene delivery using synthetic vectors. Adv Genet 53PA:19–46
3. Burton EA, Fink DJ, Glorioso JC (2002) Gene delivery using herpes simplex virus vectors. DNA Cell Biol 21:915–936
4. Campbell EM, Hope TJ (2005) Gene therapy progress and prospects: viral trafficking during infection. Gene Ther 12:1353–1359
5. Carter PJ, Samulski RJ (2000) Adeno-associated viral vectors as gene delivery vehicles. Int J Mol Med 6:17–27
6. Duan Y, Zhang S, Wang B, Yang B, Zhi D (2009) The biological routes of gene delivery mediated by lipid-based non-viral vectors. Expert Opin Drug Deliv 6:1351–1361
7. Liu F, Huang L (2002) Development of non-viral vectors for systemic gene delivery. J Control Release 78:259–266
8. Niidome T, Huang L (2002) Gene therapy progress and prospects: nonviral vectors. Gene Ther 9:1647–1652
9. Park TG, Jeong JH, Kim SW (2006) Current status of polymeric gene delivery systems. Adv Drug Deliv Rev 58:467–486
10. Schaffert D, Wagner E (2008) Gene therapy progress and prospects: synthetic polymer-based systems. Gene Ther 15:1131–1138
11. Wagner E (2004) Strategies to improve DNA polyplexes for in vivo gene transfer: will "artificial viruses" be the answer? Pharm Res 21:8–14
12. Brandenburg B, Zhuang X (2007) Virus trafficking – learning from single-virus tracking. Nat Rev Microbiol 5:197–208
13. Lakadamyali M, Rust MJ, Babcock HP, Zhuang X (2003) Visualizing infection of individual influenza viruses. Proc Natl Acad Sci USA 100:9280–9285
14. Marsh M, Helenius A (2006) Virus entry: open sesame. Cell 124:729–740
15. Seisenberger G, Ried MU, Endress T, Buning H, Hallek M, Bräuchle C (2001) Real-time single-molecule imaging of the infection pathway of an adeno-associated virus. Science 294:1929–1932

16. Khalil IA, Kogure K, Akita H, Harashima H (2006) Uptake pathways and subsequent intracellular trafficking in nonviral gene delivery. Pharmacol Rev 58:32–45
17. Medina-Kauwe LK, Xie J, Hamm-Alvarez S (2005) Intracellular trafficking of nonviral vectors. Gene Ther 12:1734–1751
18. Payne CK (2007) Imaging gene delivery with fluorescence microscopy. Nanomed 2:847–860
19. Watson P, Jones AT, Stephens DJ (2005) Intracellular trafficking pathways and drug delivery: fluorescence imaging of living and fixed cells. Adv Drug Deliv Rev 57:43–61
20. Vercauteren D et al (2010) The use of inhibitors to study endocytic pathways of gene carriers: optimization and pitfalls. Mol Ther 18:561–569
21. Rejman J, Bragonzi A, Conese M (2005) Role of clathrin- and caveolae-mediated endocytosis in gene transfer mediated by lipo- and polyplexes. Mol Ther 12:468–474
22. Remy-Kristensen A, Clamme JP, Vuilleumier C, Kuhry JG, Mely Y (2001) Role of endocytosis in the transfection of L929 fibroblasts by polyethylenimine/DNA complexes. Biochim Biophys Acta 1514:21–32
23. Kopatz I, Remy JS, Behr JP (2004) A model for non-viral gene delivery: through syndecan adhesion molecules and powered by actin. J Gene Med 6:769–776
24. Lundin P, Johansson H, Guterstam P, Holm T, Hansen M, Langel U, EL Andaloussi S (2008) Distinct uptake routes of cell-penetrating peptide conjugates. Bioconjug Chem 19:2535–2542
25. Mae M, Andaloussi SE, Lehto T, Langel U (2009) Chemically modified cell-penetrating peptides for the delivery of nucleic acids. Expert Opin Drug Deliv 6:1195–1205
26. Rinne J, Albarran B, Jylhava J, Ihalainen TO, Kankaanpaa P, Hytonen VP, Stayton PS, Kulomaa MS, Vihinen-Ranta M (2007) Internalization of novel non-viral vector TAT-streptavidin into human cells. BMC Biotechnol 7:1
27. von Gersdorff K, Sanders NN, Vandenbroucke R, De Smedt SC, Wagner E, Ogris M (2006) The internalization route resulting in successful gene expression depends on both cell line and polyethylenimine polyplex type. Mol Ther 14:745–753
28. Benns JM, Kim SW (2000) Tailoring new gene delivery designs for specific targets. J Drug Target 8:1–12
29. Cheng H, Zhu JL, Zeng X, Jing Y, Zhang XZ, Zhuo RX (2009) Targeted gene delivery mediated by folate-polyethylenimine-block-poly(ethylene glycol) with receptor selectivity. Bioconjug Chem 20:481–487
30. Lu T, Sun J, Chen X, Zhang P, Jing X (2009) Folate-conjugated micelles and their folate-receptor-mediated endocytosis. Macromol Biosci 9:1059–1068
31. Frederiksen KS, Abrahamsen N, Cristiano RJ, Damstrup L, Poulsen HS (2000) Gene delivery by an epidermal growth factor/DNA polyplex to small cell lung cancer cell lines expressing low levels of epidermal growth factor receptor. Cancer Gene Ther 7:262–268
32. Godinez WJ, Lampe M, Worz S, Muller B, Eils R, Rohr K (2009) Deterministic and probabilistic approaches for tracking virus particles in time-lapse fluorescence microscopy image sequences. Med Image Anal 13:325–342
33. Sbalzarini IF, Koumoutsakos P (2005) Feature point tracking and trajectory analysis for video imaging in cell biology. J Struct Biol 151:182–195
34. Yildiz A, Forkey JN, McKinney SA, Ha T, Goldman YE, Selvin PR (2003) Myosin V walks hand-over-hand: single fluorophore imaging with 1.5-nm localization. Science 300:2061–2065
35. Saxton MJ, Jacobson K (1997) Single-particle tracking: applications to membrane dynamics. Annu Rev Biophys Biomol Struct 26:373–399
36. Qian H, Sheetz MP, Elson EL (1991) Single particle tracking. Analysis of diffusion and flow in two-dimensional systems. Biophys J 60:910–921
37. de Bruin K, Ruthardt N, von Gersdorff K, Bausinger R, Wagner E, Ogris M, Bräuchle C (2007) Cellular dynamics of EGF receptor-targeted synthetic viruses. Mol Ther 15:1297–1305
38. Bausinger R, von Gersdorff K, Braeckmans K, Ogris M, Wagner E, Bräuchle C, Zumbusch A (2006) The transport of nanosized gene carriers unraveled by live-cell imaging. Angew Chem Int Ed Engl 45:1568–1572

39. Mislick KA, Baldeschwieler JD (1996) Evidence for the role of proteoglycans in cation-mediated gene transfer. Proc Natl Acad Sci USA 93:12349–12354
40. Payne CK, Jones SA, Chen C, Zhuang X (2007) Internalization and trafficking of cell surface proteoglycans and proteoglycan-binding ligands. Traffic 8:389–401
41. Suh J, Wirtz D, Hanes J (2004) Real-time intracellular transport of gene nanocarriers studied by multiple particle tracking. Biotechnol Prog 20:598–602
42. Cui B, Wu C, Chen L, Ramirez A, Bearer EL, Li WP, Mobley WC, Chu S (2007) One at a time, live tracking of NGF axonal transport using quantum dots. Proc Natl Acad Sci USA 104:13666–13671
43. Fehrenbacher K, Huckaba T, Yang HC, Boldogh I, Pon L (2003) Actin comet tails, endosomes and endosymbionts. J Exp Biol 206:1977–1984
44. Merrifield CJ, Moss SE, Ballestrem C, Imhof BA, Giese G, Wunderlich I, Almers W (1999) Endocytic vesicles move at the tips of actin tails in cultured mast cells. Nat Cell Biol 1:72–74
45. Mahowald J, Arcizet D, Heinrich D (2009) Impact of external stimuli and cell micro-architecture on intracellular transport states. Chemphyschem 10:1559–1566
46. Arcizet D, Meier B, Sackmann E, Rädler JO, Heinrich D (2008) Temporal analysis of active and passive transport in living cells. Phys Rev Lett 101:248103
47. Suh J, Wirtz D, Hanes J (2003) Efficient active transport of gene nanocarriers to the cell nucleus. Proc Natl Acad Sci USA 100:3878–3882
48. Sauer AM, de Bruin KG, Ruthardt N, Mykhaylyk O, Plank C, Bräuchle C (2009) Dynamics of magnetic lipoplexes studied by single-particle tracking in living cells. J Control Release 137:136–145
49. Rajan SS, Liu HY, Vu TQ (2008) Ligand-bound quantum dot probes for studying the molecular scale dynamics of receptor endocytic trafficking in live cells. ACS Nano 2:1153–1166
50. Nan X, Sims PA, Chen P, Xie XS (2005) Observation of individual microtubule motor steps in living cells with endocytosed quantum dots. J Phys Chem B 109:24220–24224
51. Lechardeur D, Verkman AS, Lukacs GL (2005) Intracellular routing of plasmid DNA during non-viral gene transfer. Adv Drug Deliv Rev 57:755–767
52. Klemm AR, Young D, Lloyd JB (1998) Effects of polyethyleneimine on endocytosis and lysosome stability. Biochem Pharmacol 56:41–46
53. Sonawane ND, Szoka FC Jr, Verkman AS (2003) Chloride accumulation and swelling in endosomes enhances DNA transfer by polyamine-DNA polyplexes. J Biol Chem 278:44826–44831
54. Clamme JP, Krishnamoorthy G, Mely Y (2003) Intracellular dynamics of the gene delivery vehicle polyethylenimine during transfection: investigation by two-photon fluorescence correlation spectroscopy. Biochim Biophys Acta 1617:52–61
55. Boeckle S, Fahrmeir J, Roedl W, Ogris M, Wagner E (2006) Melittin analogs with high lytic activity at endosomal pH enhance transfection with purified targeted PEI polyplexes. J Control Release 112:240–248
56. Ogris M, Carlisle RC, Bettinger T, Seymour LW (2001) Melittin enables efficient vesicular escape and enhanced nuclear access of nonviral gene delivery vectors. J Biol Chem 276:47550–47555
57. de Bruin KG, Fella C, Ogris M, Wagner E, Ruthardt N, Bräuchle C (2008) Dynamics of photoinduced endosomal release of polyplexes. J Control Release 130:175–182
58. Lukacs GL, Haggie P, Seksek O, Lechardeur D, Freedman N, Verkman AS (2000) Size-dependent DNA mobility in cytoplasm and nucleus. J Biol Chem 275:1625–1629
59. Vaughan EE, Dean DA (2006) Intracellular trafficking of plasmids during transfection is mediated by microtubules. Mol Ther 13:422–428
60. Leopold PL, Kreitzer G, Miyazawa N, Rempel S, Pfister KK, Rodriguez-Boulan E, Crystal RG (2000) Dynein- and microtubule-mediated translocation of adenovirus serotype 5 occurs after endosomal lysis. Hum Gene Ther 11:151–165

61. Dohner K, Radtke K, Schmidt S, Sodeik B (2006) Eclipse phase of herpes simplex virus type 1 infection: efficient dynein-mediated capsid transport without the small capsid protein VP26. J Virol 80:8211–8224
62. Dohner K, Wolfstein A, Prank U, Echeverri C, Dujardin D, Vallee R, Sodeik B (2002) Function of dynein and dynactin in herpes simplex virus capsid transport. Mol Biol Cell 13:2795–2809
63. Suk JS, Suh J, Lai SK, Hanes J (2007) Quantifying the intracellular transport of viral and nonviral gene vectors in primary neurons. Exp Biol Med (Maywood) 232:461–469
64. Matsumoto Y, Itaka K, Yamasoba T, Kataoka K (2009) Intranuclear fluorescence resonance energy transfer analysis of plasmid DNA decondensation from nonviral gene carriers. J Gene Med 11:615–623
65. Godbey WT, Barry MA, Saggau P, Wu KK, Mikos AG (2000) Poly(ethylenimine)-mediated transfection: a new paradigm for gene delivery. J Biomed Mater Res 51:321–328
66. Godbey WT, Wu KK, Mikos AG (1999) Tracking the intracellular path of poly(ethylenimine)/DNA complexes for gene delivery. Proc Natl Acad Sci USA 96:5177–5181
67. Itaka K, Harada A, Yamasaki Y, Nakamura K, Kawaguchi H, Kataoka K (2004) In situ single cell observation by fluorescence resonance energy transfer reveals fast intra-cytoplasmic delivery and easy release of plasmid DNA complexed with linear polyethylenimine. J Gene Med 6:76–84
68. Bieber T, Meissner W, Kostin S, Niemann A, Elsasser HP (2002) Intracellular route and transcriptional competence of polyethylenimine-DNA complexes. J Control Release 82: 441–454
69. Brunner S, Sauer T, Carotta S, Cotten M, Saltik M, Wagner E (2000) Cell cycle dependence of gene transfer by lipoplex, polyplex and recombinant adenovirus. Gene Ther 7:401–407
70. Mortimer I, Tam P, MacLachlan I, Graham RW, Saravolac EG, Joshi PB (1999) Cationic lipid-mediated transfection of cells in culture requires mitotic activity. Gene Ther 6:403–411
71. Tseng WC, Haselton FR, Giorgio TD (1999) Mitosis enhances transgene expression of plasmid delivered by cationic liposomes. Biochim Biophys Acta 1445:53–64
72. Schwake G, Youssef S, Kuhr JT, Gude S, David MP, Mendoza E, Frey E, Rädler JO (2009) Predictive modeling of non-viral gene transfer. Biotechnol Bioeng 105:805–813
73. Cohen RN, van der Aa MA, Macaraeg N, Lee AP, Szoka FC Jr (2009) Quantification of plasmid DNA copies in the nucleus after lipoplex and polyplex transfection. J Control Release 135:166–174
74. Holtzer L, Meckel T, Schmidt T (2007) Nanometric three-dimensional tracking of individual quantum dots in cells. Appl Phys Lett 90:1–3
75. Katayama Y, Burkacky O, Meyer M, Bräuchle C, Gratton E, Lamb DC (2009) Real-time nanomicroscopy via three-dimensional single-particle tracking. Chemphyschem 10:2458–2464
76. Wagner E (2007) Programmed drug delivery: nanosystems for tumor targeting. Expert Opin Biol Ther 7:587–593
77. Zintchenko A, Susha AS, Concia M, Feldmann J, Wagner E, Rogach AL, Ogris M (2009) Drug nanocarriers labeled with near-infrared-emitting quantum dots (quantoplexes): imaging fast dynamics of distribution in living animals. Mol Ther 17:1849–1856